

First Simultaneous Determination of Inclusive and Exclusive $|V_{ub}|$

L. Cao^{*}, F. Bernlochner[†], K. Tackmann, I. Adachi, H. Aihara, S. Al Said, D. M. Asner, H. Atmacan, T. Aushev, R. Ayad, V. Babu, S. Bahinipati, Sw. Banerjee, P. Behera, K. Belous, J. Bennett, M. Bessner, B. Bhuyan, T. Bilka, D. Biswas, A. Bobrov, D. Bodrov, J. Borah, A. Bozek, M. Bračko, P. Branchini, T. E. Browder, A. Budano, M. Campajola, D. Červakov, M.-C. Chang, B. G. Cheon, K. Chilikin, H. E. Cho, K. Cho, S.-J. Cho, S.-K. Choi, Y. Choi, S. Choudhury, D. Cinabro, S. Cunliffe, S. Das, G. de Marino, G. De Nardo, G. De Pietro, R. Dhamija, F. Di Capua, J. Dingfelder, Z. Doležal, T. V. Dong, T. Ferber, D. Ferlewicz, B. G. Fulsom, V. Gaur, A. Garmash, A. Giri, P. Goldenzweig, E. Graziani, T. Gu, Y. Guan, K. Gudkova, C. Hadjivasiliou, S. Halder, T. Hara, O. Hartbrich, K. Hayasaka, H. Hayashii, M. T. Hedges, D. Herrmann, W.-S. Hou, C.-L. Hsu, T. Iijima, K. Inami, N. Ipsita, A. Ishikawa, R. Itoh, M. Iwasaki, W. W. Jacobs, E.-J. Jang, S. Jia, Y. Jin, K. K. Joo, D. Kalita, K. H. Kang, C. Kiesling, C. H. Kim, D. Y. Kim, K.-H. Kim, Y.-K. Kim, K. Kinoshita, P. Kodyš, T. Konno, A. Korobov, S. Korpar, E. Kovalenko, P. Križan, P. Krokovny, T. Kuhr, R. Kumar, K. Kumara, A. Kuzmin, Y.-J. Kwon, J. S. Lange, M. Laurenza, S. C. Lee, P. Lewis, J. Li, L. K. Li, Y. Li, J. Libby, Y.-R. Lin, D. Liventsev, T. Luo, Y. Ma, A. Martini, M. Masuda, T. Matsuda, D. Matvienko, S. K. Maurya, F. Meier, M. Merola, F. Metzner, K. Miyabayashi, R. Mizuk, G. B. Mohanty, M. Mrvar, R. Mussa, I. Nakamura, M. Nakao, Z. Natkaniec, A. Natochii, L. Nayak, M. Nayak, N. K. Nisar, S. Nishida, K. Ogawa, S. Ogawa, H. Ono, P. Oskin, P. Pakhlov, G. Pakhlova, T. Pang, S. Pardi, H. Park, J. Park, S.-H. Park, A. Passeri, S. Patra, S. Paul, T. K. Pedlar, R. Pestotnik, L. E. Piilonen, T. Podobnik, E. Prencipe, M. T. Prim, N. Rout, M. Rozanska, G. Russo, S. Sandilya, A. Sangal, L. Santelj, V. Savinov, G. Schnell, C. Schwanda, Y. Seino, K. Senyo, M. E. Sevier, W. Shan, M. Shapkin, C. Sharma, C. P. Shen, J.-G. Shiu, B. Shwartz, A. Sokolov, E. Solovieva, M. Starič, Z. S. Stottler, M. Sumihama, W. Sutcliffe, M. Takizawa, U. Tamponi, K. Tanida, F. Tenchini, R. Tiwary, K. Trabelsi, M. Uchida, T. Uglov, Y. Unno, K. Uno, S. Uno, Y. Ushiroda, Y. Usov, S. E. Vahsen, G. Varner, K. E. Varvell, A. Vossen, D. Wang, E. Wang, M.-Z. Wang, S. Watanuki, O. Werbycka, E. Won, X. Xu, B. D. Yabsley, W. Yan, S. B. Yang, J. H. Yin, Y. Yook, Y. Yusa, Z. P. Zhang, V. Zhilich, and V. Zhukova
(The Belle Collaboration)

The first simultaneous determination of the absolute value of the Cabibbo-Kobayashi-Maskawa matrix element V_{ub} using inclusive and exclusive decays is performed with the full Belle data set at the $\Upsilon(4S)$ resonance, corresponding to an integrated luminosity of 711 fb^{-1} . We analyze collision events in which one B meson is fully reconstructed in hadronic modes. This allows for the reconstruction of the hadronic X_u system of the semileptonic $b \rightarrow u \ell \bar{\nu}_\ell$ decay. We separate exclusive $B \rightarrow \pi \ell \bar{\nu}_\ell$ decays from other inclusive $B \rightarrow X_u \ell \bar{\nu}_\ell$ and backgrounds with a two-dimensional fit, that utilizes the number of charged pions in the X_u system and the four-momentum transfer q^2 between the B and X_u system. Combining our measurement with information from lattice QCD and QCD calculations of the inclusive partial rate as well as external experimental information on the shape of the $B \rightarrow \pi \ell \bar{\nu}_\ell$ form factor, we determine $|V_{ub}^{\text{excl.}}| = (3.78 \pm 0.23 \pm 0.16 \pm 0.14) \times 10^{-3}$ and $|V_{ub}^{\text{incl.}}| = (3.90 \pm 0.20 \pm 0.32 \pm 0.09) \times 10^{-3}$, respectively, with the uncertainties being the statistical error, systematic errors, and theory errors. The ratio of $|V_{ub}^{\text{excl.}}|/|V_{ub}^{\text{incl.}}| = 0.97 \pm 0.12$ is compatible with unity.

PACS numbers: 12.15.Hh, 13.20.-v, 14.40.Nd

In this letter we report the first simultaneous determination of the absolute value of the Cabibbo-Kobayashi-Maskawa (CKM) matrix element V_{ub} using inclusive and exclusive decays. Exclusive determinations of $|V_{ub}|$ focus on reconstructing explicit final states such as $B \rightarrow \pi \ell \bar{\nu}_\ell$ [1], $\Lambda_b \rightarrow p \mu \bar{\nu}_\mu$ [2], or $B_s \rightarrow K \mu \bar{\nu}_\mu$ [3], whereas inclusive determinations study B meson decays undergoing $b \rightarrow u \ell \bar{\nu}_\ell$ transitions and are indiscriminate of the

$u \rightarrow X_u$ hadronization process. The world averages of either method are only marginally compatible [1],

$$|V_{ub}^{\text{excl.}}| = (3.51 \pm 0.12) \times 10^{-3}, \quad (1)$$

$$|V_{ub}^{\text{incl.}}| = (4.19 \pm 0.16) \times 10^{-3}, \quad (2)$$

with a ratio of $|V_{ub}^{\text{excl.}}|/|V_{ub}^{\text{incl.}}| = 0.84 \pm 0.04$, which deviates 3.7 standard deviations from unity. The underlying

reason for this tension is unknown. New physics explanations are challenging (see e.g. Refs. [4–7]), leading to some to speculate the existence of until now unaccounted systematic effects [8]. This motivates the simultaneous determination in a single analysis.

The presented measurement of inclusive and exclusive $b \rightarrow u\ell\bar{\nu}_\ell$ decays uses the same collision events and a similar analysis strategy as Refs. [9, 10]. Charmless semileptonic decays are reconstructed by relying on the complete reconstruction of the second B meson in the $e^+e^- \rightarrow \Upsilon(4S) \rightarrow B\bar{B}$ process. This approach allows for the direct reconstruction of the X_u system of the $B \rightarrow X_u\ell\bar{\nu}_\ell$ process. Specifically, the four-momentum transfer squared, $q^2 = (p_B - p_{X_u})^2$, and the number of charged pion candidates of the X_u system, N_{π^\pm} , can be reconstructed. This allows for the separation of $B^+ \rightarrow \pi^0\ell^+\nu_\ell$ and $B^0 \rightarrow \pi^-\ell^+\nu_\ell$ from other $B \rightarrow X_u\ell\bar{\nu}_\ell$ decays. The main background in the measurement stems from the much more abundant $B \rightarrow X_c\ell\bar{\nu}_\ell$ decays and a multivariate suppression strategy is used to reduce this and other background processes. Charge conjugation is implied throughout. The inclusive $B \rightarrow X_u\ell\bar{\nu}_\ell$ branching fraction is defined as the average branching fraction of B^+ and B^0 meson decays. Furthermore, we denote $\ell = e, \mu$, and use natural units: $\hbar = c = 1$.

We analyze $(772 \pm 10) \times 10^6$ B meson pairs recorded at the $\Upsilon(4S)$ resonance energy and 79fb^{-1} of collision events recorded 60 MeV below the $\Upsilon(4S)$ peak. Both data sets were recorded at the KEKB e^+e^- collider [11] by the Belle detector. Belle is a large-solid-angle magnetic spectrometer. A detailed description of its performance and subdetectors can be found in Ref. [12]. The particle identification and selection criteria are the same as in Ref. [9].

Monte Carlo (MC) samples of B meson decays and continuum processes ($e^+e^- \rightarrow q\bar{q}$ with $q = u, d, s, c$) are simulated using the **EvtGen** generator [13]. The normalization of continuum events is calibrated with the measured off-resonance data. A detailed description of all samples and decay models is given in Ref. [9]. The simulated samples are used for background subtraction and to correct for detector resolution, selection, and acceptance effects. The used sample sizes correspond to approximately ten and five times, respectively, the Belle collision data for the B meson production and continuum processes.

Semileptonic $B \rightarrow X_u\ell\bar{\nu}_\ell$ decays are simulated as a mixture of specific exclusive modes and nonresonant contributions using a “hybrid” approach [14–16]: the triple differential rate of inclusive and exclusive predictions are combined such that the partial rates of the inclusive prediction are recovered. This is achieved by assigning weights to the inclusive contribution as a function of the generator-level q^2 , E_ℓ^B , and M_X . Here E_ℓ^B and M_X denote the energy of the lepton in the signal B rest frame and the invariant mass of the X_u system

produced in the $B \rightarrow X_u\ell\bar{\nu}_\ell$ decay. For the inclusive contribution, we use two different calculations: the De Fazio and Neubert (DFN) model [17] (with $m_b^{\text{KN}} = (4.66 \pm 0.04)\text{ GeV}$, $a^{\text{KN}} = 1.3 \pm 0.5$) and the Bosch-Lange-Neubert-Paz (BLNP) model [18] (with $m_b^{\text{SF}} = 4.61\text{ GeV}$, $\mu_\pi^{2\text{SF}} = 0.20\text{ GeV}^2$). The difference between the two models is treated as a systematic uncertainty. The simulated inclusive $B \rightarrow X_u\ell\bar{\nu}_\ell$ events are hadronized with the JETSET algorithm [19] into final states with two or more mesons. We study two different tunes of the fragmentation parameters and assign their difference as a systematic uncertainty. The exclusive contributions are modeled as follows: $B \rightarrow \pi\ell\bar{\nu}_\ell$ decays are modeled using the Bourrely-Caprini-Lellouch (BCL) form factor parameterization [20]; $B \rightarrow \rho\ell\bar{\nu}_\ell$ and $B \rightarrow \omega\ell\bar{\nu}_\ell$ decays are modeled using the Bharucha-Straub-Zwicky (BSZ) form factors [21] from the fit of Ref. [22] to light-cone sum rule (LCSR) predictions [21] and the measurements of Refs. [23–25]; $B \rightarrow \eta\ell\bar{\nu}_\ell$ and $B \rightarrow \eta'\ell\bar{\nu}_\ell$ are modeled using pole form factors obtained from fits to LCSR [26]. For the branching fractions the world averages from Ref. [27] are used.

Semileptonic $B \rightarrow X_c\ell\bar{\nu}_\ell$ decays are dominated by $B \rightarrow D\ell\bar{\nu}_\ell$ and $B \rightarrow D^*\ell\bar{\nu}_\ell$ decays. We simulate them with the form factors of Refs. [28–30] and values determined by the measurements of Refs. [31, 32]. Other $B \rightarrow X_c\ell\bar{\nu}_\ell$ decays are simulated as a mixture of resonant and nonresonant modes, using the parameterization of Ref. [33] for the modeling of $B \rightarrow D^{**}\ell\bar{\nu}_\ell$ form factors. The known difference between inclusive and the sum of measured exclusive $B \rightarrow X_c\ell\bar{\nu}_\ell$ decays is simulated with $B \rightarrow D^{(*)}\eta\ell^+\nu_\ell$ decays.

We reconstruct e^+e^- collision events with the multivariate tagging algorithm of Ref. [34]. The algorithm uses a hierarchical approach utilizing neural networks to fully reconstruct one of the two B mesons in hadronic final states (labeled as B_{tag}). The B_{tag} reconstruction efficiency is calibrated using $B \rightarrow X_c\ell\bar{\nu}_\ell$ decays following the prescription outlined in [9]. The identified final state particles forming the B_{tag} are masked and $b \rightarrow u\ell\bar{\nu}_\ell$ signal candidates are reconstructed by identifying an electron or muon candidate in the events, requiring $E_\ell^B = |\mathbf{p}_\ell^B| > 1\text{ GeV}$ as measured in the signal B rest frame. To reject background from the much more abundant $B \rightarrow X_c\ell\bar{\nu}_\ell$ decays, eleven distinguishing features are combined into a single discriminant using boosted decision trees (BDTs) and utilizing the implementation of Ref. [35]. The most discriminating training features are the reconstructed neutrino mass, M_{miss}^2 , the vertex fit probability of the decay vertex between the hadronic system X and the signal lepton ℓ , and the number of identified K^\pm and K_S^0 in the X system. Same as in [9], we select a working point that corresponds to a signal efficiency of 18.5%, which rejects 98.7% of $B \rightarrow X_c\ell\bar{\nu}_\ell$ decays, defined with respect to all events after the B_{tag} selection. To test the modeling

of $B \rightarrow X_c \ell \bar{\nu}_\ell$ and other backgrounds in the extraction variables, q^2 and N_{π^\pm} , we also utilize the events failing the BDT selection and find good agreement. We further separate events by the reconstructed M_X , categorizing $M_X < 1.7 \text{ GeV}$ into five q^2 bins ranging in $[0, 26.4] \text{ GeV}^2$ as a function of the N_{π^\pm} multiplicity for the interval of $[0, 1, 2, \geq 3]$. Events with $M_X \geq 1.7 \text{ GeV}$ are analyzed only in bins of N_{π^\pm} as they are dominated by background. To enhance the $B \rightarrow \pi \ell \bar{\nu}_\ell$ purity in the low- M_X $N_{\pi^\pm} = 0$ and $N_{\pi^\pm} = 1$ events, we apply a selection on the thrust of 0.92 and 0.85, respectively. It is defined by $\max_{|\mathbf{n}|=1} (\sum_i |\mathbf{p}_i \cdot \mathbf{n}| / \sum_i |\mathbf{p}_i|)$, when summing over the neutral and charged constituents of the reconstructed X system in the center of mass frame. For $B \rightarrow \pi \ell \bar{\nu}_\ell$ events, we expect a more collimated X_u system than for $B \rightarrow X_c \ell \bar{\nu}_\ell$ and other $B \rightarrow X_u \ell \bar{\nu}_\ell$ processes, resulting in a higher thrust value.

The $q^2 : N_{\pi^\pm}$ bins and the $M_X \geq 1.7 \text{ GeV}$ N_{π^\pm} distribution are analyzed using a simultaneous likelihood fit, which incorporates floating parameters for the modeling of the $B \rightarrow \pi \ell \bar{\nu}_\ell$ form factor, the binned templates, and systematic uncertainties as nuisance parameters. Specifically, the shape of $B \rightarrow \pi \ell \bar{\nu}_\ell$ template is linked to the form factors by correcting the efficiency and acceptance effects. The fit components we probe are the normalizations of $B \rightarrow \pi \ell \bar{\nu}_\ell$ decays, other $B \rightarrow X_u \ell \bar{\nu}_\ell$ signal decays, and of background events dominated by $B \rightarrow X_c \ell \bar{\nu}_\ell$ decays. The f_+ and f_0 form factors describing the $B \rightarrow \pi \ell \bar{\nu}_\ell$ decay dynamics are parameterized with expansion coefficients a_n^+ and a_n^0 using the BCL expansion,

$$f_+(q^2) = \frac{1}{1 - q^2/m_{B^*}^2} \sum_{n=0}^{N^+-1} a_n^+ \left[z^n - (-1)^{n-N^+} \frac{n}{N^+} z^{N^+} \right],$$

$$f_0(q^2) = \sum_{n=0}^{N^0-1} a_n^0 z^n, \quad (3)$$

at expansion order $N^+ = N^0 = 3$ in the conformal variable $z = z(q^2)$ [20, 36], and a_2^0 is expressed by the remaining coefficients to keep the kinematical constraint $f_+(0) = f_0(0)$. We constrain the expansion coefficients to the lattice QCD (LQCD) values of Ref. [36], combining LQCD calculations from several groups [37, 38]. Note that the measured distributions have no sensitivity for f_0 and we thus neglect its effects in the decay rate. The inclusion of the f_0 expansion coefficients, however, reduces uncertainties on the $B \rightarrow \pi \ell \bar{\nu}_\ell$ rate through the correlation to the f_+ shape. We also study a fit scenario that constrains the $B \rightarrow \pi$ form factors to the combined lattice QCD and experimental information of Refs. [39–42], representing the full experimental knowledge of its shape to date.

We consider additive and multiplicative systematic uncertainties in the likelihood fit by adding bin-wise nuisance parameters for each template. The parameters are

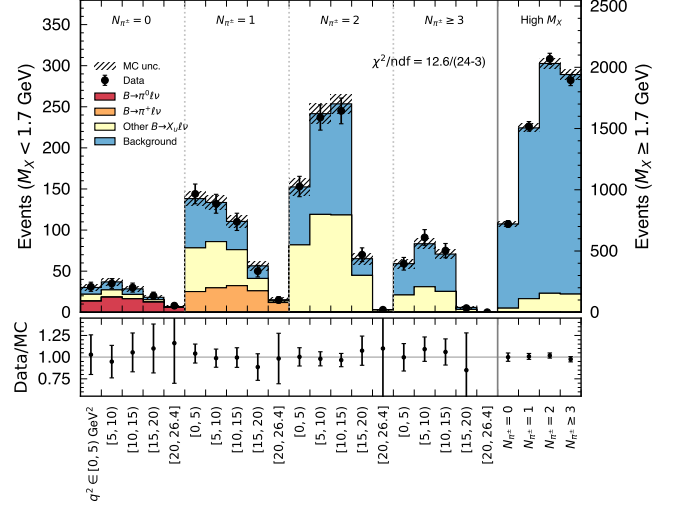


FIG. 1. The $q^2 : N_{\pi^\pm}$ spectrum after the 2D fit is shown for the scenario that only uses LQCD information. The uncertainties incorporate all postfit uncertainties discussed in the text.

constrained to a multinormal Gaussian distribution with a covariance reflecting the sum of all considered systematic effects, and the correlation structure between templates from common sources is taken into account. This includes detector and reconstruction related uncertainties, such as the tracking efficiency for low and high momentum tracks, particle identification efficiency uncertainties, and the calibration of the B_{tag} reconstruction efficiency. We further consider uncertainties on the $B \rightarrow X_u \ell \bar{\nu}_\ell$ and $B \rightarrow X_c \ell \bar{\nu}_\ell$ shapes from the form factors, non-perturbative parameters, and their compositions. The $u \rightarrow X_u$ fragmentation uncertainties are evaluated by changing the default Belle tune of fragmentation parameters to the values used in Ref. [43]. We further vary the $s\bar{s}$ -production rate $\gamma_s = 0.30 \pm 0.09$, spanning the range of Refs. [44, 45]. The largest uncertainties on the exclusive branching fraction measurements are from the calibration of the tagging efficiency ($\pm 4.0\%$) and the $B \rightarrow X_u \ell \bar{\nu}_\ell$ modeling ($\pm 3.5\%$). The largest uncertainties on the inclusive branching fraction measurement are from the $B \rightarrow X_u \ell \bar{\nu}_\ell$ ($\pm 12.1\%$) modeling and the $u \rightarrow X_u$ fragmentation ($\pm 5.3\%$). The uncertainties of the modeling of the $B \rightarrow X_c \ell \bar{\nu}_\ell$ background are $\pm 1.2\%$ and $\pm 2.8\%$ for the $B \rightarrow \pi \ell \bar{\nu}_\ell$ and $B \rightarrow X_u \ell \bar{\nu}_\ell$ branching fractions, respectively.

Figure 1 shows the $q^2 : N_{\pi^\pm}$ distribution of the signal region after the fit and with only using LQCD information: $B^+ \rightarrow \pi^0 \ell^+ \nu_\ell$ and $B^0 \rightarrow \pi^- \ell^+ \nu_\ell$ events are aggregated in the $N_{\pi^+} = 0$ and $N_{\pi^+} = 1$ bins, respectively, whereas contributions from other $B \rightarrow X_u \ell \bar{\nu}_\ell$ processes are in all multiplicity bins. The high M_X bins constrain the $B \rightarrow X_c \ell \bar{\nu}_\ell$ and other background contributions. We use the isospin relation and B^0/B^+ lifetime ratio to link

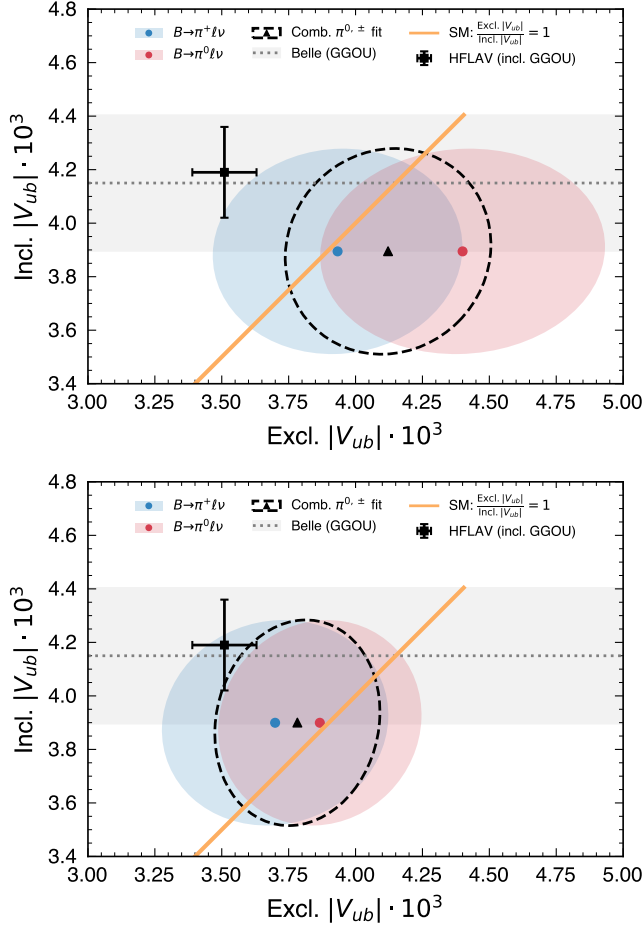


FIG. 2. The $|V_{ub}|$ values obtained with the fits using (top) LQCD or (bottom) LQCD and experimental constraints for the $\bar{B}^0 \rightarrow \pi^+ \ell^- \bar{\nu}_\ell$ form factor are shown. The inclusive $|V_{ub}|$ value is based on the decay rate from the GGOU calculation. The values obtained from the previous Belle measurement [9] (grey band) and the world averages from Ref. [1] (black marker) are also shown. The shown ellipses correspond to 39.3% confidence levels ($\Delta\chi^2 = 1$).

the yields of $B^+ \rightarrow \pi^0 \ell^+ \nu_\ell$ and $B^0 \rightarrow \pi^- \ell^+ \nu_\ell$. The fit has a χ^2 of 12.6 with 21 degrees of freedom, corresponding to a p-value of 92%. The measured $B^+ \rightarrow \pi^0 \ell^+ \nu_\ell$ and $B^0 \rightarrow \pi^- \ell^+ \nu_\ell$ yields are corrected for efficiency effects to determine the corresponding branching fractions \mathcal{B} . The measured inclusive yield is calculated from the sum of $B^+ \rightarrow \pi^0 \ell^+ \nu_\ell$, $B^0 \rightarrow \pi^- \ell^+ \nu_\ell$, and other $B \rightarrow X_u \ell \bar{\nu}_\ell$ events and unfolded to correspond to a partial branching fraction $\Delta\mathcal{B}$ with $E_\ell^B > 1.0$ GeV, also correcting for the effect of final state radiation photons. We find

$$\mathcal{B}(\bar{B}^0 \rightarrow \pi^+ \ell^- \bar{\nu}_\ell) = (1.43 \pm 0.19 \pm 0.13) \times 10^{-4}, \quad (4)$$

$$\Delta\mathcal{B}(B \rightarrow X_u \ell \bar{\nu}_\ell) = (1.40 \pm 0.14 \pm 0.23) \times 10^{-3}, \quad (5)$$

with the errors denoting statistical and systematic uncertainties. The recovered branching fraction for

$\bar{B}^0 \rightarrow \pi^+ \ell^- \bar{\nu}_\ell$ is compatible with the world average of $\mathcal{B}(\bar{B}^0 \rightarrow \pi^+ \ell^- \bar{\nu}_\ell) = (1.50 \pm 0.06) \times 10^{-4}$ [1]. The correlation between the exclusive and inclusive branching fractions is $\rho = 0.10$. Using calculations for the inclusive partial rate and the fitted form factor parameters, we can determine values for $|V_{ub}|$. As our baseline we use the GGOU [46] calculation for the inclusive partial rate with $E_\ell^B > 1.0$ GeV ($\Delta\Gamma = 58.5 \pm 2.7$ ps $^{-1}$), but other calculations result in similar values for inclusive $|V_{ub}|$. We find

$$|V_{ub}^{\text{excl.}}| = (4.12 \pm 0.30 \pm 0.18 \pm 0.16) \times 10^{-3}, \quad (6)$$

$$|V_{ub}^{\text{incl.}}| = (3.90 \pm 0.20 \pm 0.32 \pm 0.09) \times 10^{-3}, \quad (7)$$

for exclusive and inclusive $|V_{ub}|$ with the uncertainties denoting the statistical error, systematic error, and error from theory (either from LQCD or the inclusive calculation). The correlation between the exclusive and inclusive $|V_{ub}|$ is $\rho = 0.07$. The determined value for inclusive $|V_{ub}|$ is compatible with the determination of Ref. [9]. For the ratio of inclusive and exclusive V_{ub} values we find

$$|V_{ub}^{\text{excl.}}| / |V_{ub}^{\text{incl.}}| = 1.06 \pm 0.14, \quad (8)$$

which is compatible with the SM expectation of unity. The value is higher and compatible with the current world average of $|V_{ub}^{\text{excl.}}| / |V_{ub}^{\text{incl.}}| = 0.84 \pm 0.04$ [1] within 1.6 standard deviations. Fig. 2 (top) compares the measured individual values with the SM expectation and the current world average. We also test what happens if we relax the isospin relation between $B^- \rightarrow \pi^0 \ell^- \bar{\nu}_\ell$ (red ellipse) and $\bar{B}^0 \rightarrow \pi^+ \ell^- \bar{\nu}_\ell$ (blue) branching fractions and find compatible results for exclusive and inclusive $|V_{ub}|$, as well as for the exclusive $|V_{ub}|$ values.

In addition to this extraction, we can also utilize the full theoretical and experimental knowledge of the $B \rightarrow \pi \ell \bar{\nu}_\ell$ form factor, combining shape information from the measured q^2 spectrum with LQCD predictions, as provided by Ref. [36]. The determined (partial) branching fractions in this scenario are

$$\mathcal{B}(\bar{B}^0 \rightarrow \pi^+ \ell^- \bar{\nu}_\ell) = (1.53 \pm 0.18 \pm 0.12) \times 10^{-4}, \quad (9)$$

$$\Delta\mathcal{B}(B \rightarrow X_u \ell \bar{\nu}_\ell) = (1.40 \pm 0.14 \pm 0.23) \times 10^{-3}, \quad (10)$$

with a correlation of $\rho = 0.12$ between inclusive and exclusive branching fractions. This fit leads to a more precise value of $|V_{ub}|$ from $B \rightarrow \pi \ell \bar{\nu}_\ell$ and we find with the same inclusive calculation

$$|V_{ub}^{\text{excl.}}| = (3.78 \pm 0.23 \pm 0.16 \pm 0.14) \times 10^{-3}, \quad (11)$$

$$|V_{ub}^{\text{incl.}}| = (3.90 \pm 0.20 \pm 0.32 \pm 0.09) \times 10^{-3}, \quad (12)$$

with a correlation $\rho = 0.10$ and a ratio of

$$|V_{ub}^{\text{excl.}}| / |V_{ub}^{\text{incl.}}| = 0.97 \pm 0.12, \quad (13)$$

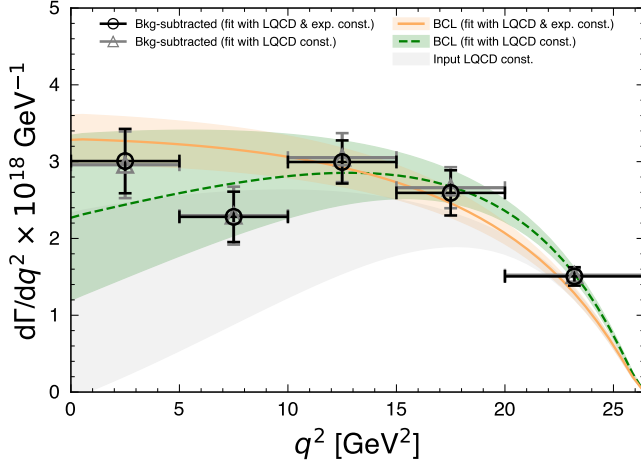


FIG. 3. The q^2 spectra of $\bar{B}^0 \rightarrow \pi^+ \ell^- \bar{\nu}_\ell$ obtained from the fit of the combined LQCD and experimental information (orange, solid) and from the fit to LQCD only (green, dashed) are shown. The data points are the background subtracted post-fit distributions, corrected for resolution and efficiency effects and averaged over both isospin modes. In addition, the LQCD pre-fit prediction of [36] for the $\bar{B}^0 \rightarrow \pi^+ \ell^- \bar{\nu}_\ell$ form factor is shown (grey).

compatible with the world average within 1.1 standard deviations. Fig. 2 (bottom) compares the obtained values and we also find good agreement between the isospin conjugate exclusive values of $|V_{ub}|$. Figure 3 compares the fitted q^2 spectra of the differential rate of $\bar{B}^0 \rightarrow \pi^+ \ell^- \bar{\nu}_\ell$ for both fit scenarios as well as for the LQCD input [36]. The inclusion of the full experimental and theoretical knowledge leads to a higher rate at low q^2 .

In summary, we presented the first simultaneous determination of inclusive and exclusive $|V_{ub}|$ within a single analysis. In the ratio of both $|V_{ub}|$ values many systematic uncertainties such as the tagging calibration or the lepton identification uncertainties cancel and one can directly test the SM expectation of unity. We recover ratios that are compatible with this expectation, but 1.6 standard deviations higher than the ratio of the current world averages of inclusive and exclusive $|V_{ub}|$. This tension is reduced to 1.1 standard deviations when including the constraint based on the full theoretical and experimental knowledge of the $B \rightarrow \pi \ell \bar{\nu}_\ell$ form factor shape. We average our inclusive and exclusive values from both approaches using LQCD or LQCD and additional experimental information and find,

$$|V_{ub}| = (4.01 \pm 0.27) \times 10^{-3}, \quad (\text{LQCD}) \quad (14)$$

$$|V_{ub}| = (3.85 \pm 0.26) \times 10^{-3}, \quad (\text{LQCD} + \text{exp.}) \quad (15)$$

respectively. These values can be compared with the expectation from CKM unitarity of Ref. [47] of $|V_{ub}^{\text{CKM}}| = (3.64 \pm 0.07) \times 10^{-3}$ and are compatible within 1.4 and 0.8 standard deviations, respectively. The

applied approach of simultaneously fitting q^2 and the number of charged pions in the X_u system will benefit from the large anticipated data set of Belle II. Additional fit scenarios and inclusive $|V_{ub}|$ values from other theory calculations of the partial rate are provided in the supplemental material [48].

This work, based on data collected using the Belle detector, which was operated until June 2010, was supported by the Ministry of Education, Culture, Sports, Science, and Technology (MEXT) of Japan, the Japan Society for the Promotion of Science (JSPS), and the Tau-Lepton Physics Research Center of Nagoya University; the German Research Foundation (DFG) Emmy-Noether Grant No. BE 6075/1-1; the Helmholtz W2/W3-116 grant; the Australian Research Council including grants DP180102629, DP170102389, DP170102204, DE220100462, DP150103061, FT130100303; Austrian Federal Ministry of Education, Science and Research (FWF) and FWF Austrian Science Fund No. P 31361-N36; the National Natural Science Foundation of China under Contracts No. 11675166, No. 11705209; No. 11975076; No. 12135005; No. 12175041; No. 12161141008; Key Research Program of Frontier Sciences, Chinese Academy of Sciences (CAS), Grant No. QYZDJ-SSW-SLH011; Project ZR2022JQ02 supported by Shandong Provincial Natural Science Foundation; the Ministry of Education, Youth and Sports of the Czech Republic under Contract No. LTT17020; the Czech Science Foundation Grant No. 22-18469S; Horizon 2020 ERC Advanced Grant No. 884719 and ERC Starting Grant No. 947006 “InterLeptons” (European Union); the Carl Zeiss Foundation, the Deutsche Forschungsgemeinschaft, the Excellence Cluster Universe, and the VolkswagenStiftung; the Department of Atomic Energy (Project Identification No. RTI 4002) and the Department of Science and Technology of India; the Istituto Nazionale di Fisica Nucleare of Italy; National Research Foundation (NRF) of Korea Grant Nos. 2016R1D1A1B02012900, 2018R1A2B3003643, 2018R1A6A1A06024970, RS202200197659, 2019R1-I1A3A01058933, 2021R1A6A1A03043957, 2021R1F1A-1060423, 2021R1F1A1064008, 2022R1A2C1003993; Radiation Science Research Institute, Foreign Large-size Research Facility Application Supporting project, the Global Science Experimental Data Hub Center of the Korea Institute of Science and Technology Information and KREONET/GLORIAD; the Polish Ministry of Science and Higher Education and the National Science Center; the Ministry of Science and Higher Education of the Russian Federation, Agreement 14.W03.31.0026, and the HSE University Basic Research Program, Moscow; University of Tabuk research grants S-1440-0321, S-0256-1438, and S-0280-1439 (Saudi Arabia); the Slovenian Research Agency Grant Nos. J1-9124 and P1-0135; Ikerbasque, Basque Foundation for Science, Spain; the

Swiss National Science Foundation; the Ministry of Education and the Ministry of Science and Technology of Taiwan; and the United States Department of Energy and the National Science Foundation. These acknowledgements are not to be interpreted as an endorsement of any statement made by any of our institutes, funding agencies, governments, or their representatives. We thank the KEKB group for the excellent operation of the accelerator; the KEK cryogenics group for the efficient operation of the solenoid; and the KEK computer group and the Pacific Northwest National Laboratory (PNNL) Environmental Molecular Sciences Laboratory (EMSL) computing group for strong computing support; and the National Institute of Informatics, and Science Information Network 6 (SINET6) for valuable network support. We are indebted to Alexander Ermakov for his pioneering work on the subject. We thank Frank Tackmann, Zoltan Ligeti, and Dean Robinson for discussions about the content of this manuscript.

* lu.cao@desy.de

† florian.bernlochner@uni-bonn.de

- [1] Y. Amhis *et al.* (HFLAV), (2022), [arXiv:2206.07501 \[hep-ex\]](#).
- [2] R. Aaij *et al.* (LHCb Collaboration), *Nature Phys.* **11**, 743 (2015), [arXiv:1504.01568 \[hep-ex\]](#).
- [3] R. Aaij *et al.* (LHCb Collaboration), *Phys. Rev. Lett.* **126**, 081804 (2021), [arXiv:2012.05143 \[hep-ex\]](#).
- [4] A. Crivellin, *Phys. Rev. D* **81**, 031301 (2010), [arXiv:0907.2461 \[hep-ph\]](#).
- [5] T. Enomoto and M. Tanaka, *Phys. Rev. D* **91**, 014033 (2015), [arXiv:1411.1177 \[hep-ph\]](#).
- [6] F. U. Bernlochner, Z. Ligeti, and S. Turczyk, *Phys. Rev. D* **90**, 094003 (2014), [arXiv:1408.2516 \[hep-ph\]](#).
- [7] H. Umeeda, (2022), [arXiv:2208.11896 \[hep-ph\]](#).
- [8] P. Zyla *et al.* (Particle Data Group, Semileptonic b-Hadron Decays, Determination of V_{cb} and V_{ub} Review), *Prog. Theor. Exp. Phys.* **2020** 083C01 (2020).
- [9] L. Cao *et al.* (Belle Collaboration), *Phys. Rev. D* **104**, 012008 (2021), [arXiv:2102.00020 \[hep-ex\]](#).
- [10] L. Cao *et al.* (Belle Collaboration), *Phys. Rev. Lett.* **127**, 261801 (2021), [arXiv:2107.13855 \[hep-ex\]](#).
- [11] S. Kurokawa and E. Kikutani, *Nucl. Instr. and Meth.* **A499**, 1 (2003), and other papers included in this Volume; T. Abe *et al.*, *Prog. Theor. Exp. Phys.* **2013**, 03A001 (2013) and references therein.
- [12] A. Abashian *et al.*, *Nucl. Instrum. Meth.* **A479**, 117 (2002), also see detector section in J. Brodzicka *et al.*, *Prog. Theor. Exp. Phys.* **2012**, 04D001 (2012).
- [13] D. J. Lange, *Nucl. Instr. and Meth.* **A462**, 152 (2001).
- [14] C. Ramirez, J. F. Donoghue, and G. Burdman, *Phys. Rev. D* **41**, 1496 (1990).
- [15] M. Prim *et al.* (Belle Collaboration), *Phys. Rev. D* **101**, 032007 (2020), [arXiv:1911.03186 \[hep-ex\]](#).
- [16] M. Prim, “b2-hive/effort v0.1.0,” (2020), doi: 10.5281/zenodo.3965699.
- [17] F. De Fazio and M. Neubert, *JHEP* **06**, 017 (1999), [arXiv:hep-ph/9905351 \[hep-ph\]](#).
- [18] B. O. Lange, M. Neubert, and G. Paz, *Phys. Rev. D* **72**, 073006 (2005), [arXiv:hep-ph/0504071](#).
- [19] T. Sjöstrand, *Comput. Phys. Commun.* **82**, 74 (1994).
- [20] C. Bourrely, I. Caprini, and L. Lellouch, *Phys. Rev. D* **79**, 013008 (2009), [Erratum: *Phys. Rev. D* **82**, 099902 (2010)], [arXiv:0807.2722 \[hep-ph\]](#).
- [21] A. Bharucha, D. M. Straub, and R. Zwicky, *JHEP* **08**, 098 (2016), [arXiv:1503.05534 \[hep-ph\]](#).
- [22] F. U. Bernlochner, M. T. Prim, and D. J. Robinson, *Phys. Rev. D* **104**, 034032 (2021), [arXiv:2104.05739 \[hep-ph\]](#).
- [23] A. Sibidanov *et al.* (Belle Collaboration), *Phys. Rev. D* **88**, 032005 (2013), [arXiv:1306.2781 \[hep-ex\]](#).
- [24] J. P. Lees *et al.* (BaBar Collaboration), *Phys. Rev. D* **87**, 032004 (2013), [Erratum: *Phys. Rev. D* **87**, no.9, 099904 (2013)], [arXiv:1205.6245 \[hep-ex\]](#).
- [25] P. del Amo Sanchez *et al.* (BaBar Collaboration), *Phys. Rev. D* **83**, 032007 (2011), [arXiv:1005.3288 \[hep-ex\]](#).
- [26] G. Duplancic and B. Melic, *JHEP* **11**, 138 (2015), [arXiv:1508.05287 \[hep-ph\]](#).
- [27] P. Zyla *et al.* (Particle Data Group), *Prog. Theor. Exp. Phys.* **2020** 083C01 (2020).
- [28] C. G. Boyd, B. Grinstein, and R. F. Lebed, *Phys. Rev. Lett.* **74**, 4603 (1995), [arXiv:hep-ph/9412324 \[hep-ph\]](#).
- [29] B. Grinstein and A. Kobach, *Phys. Lett. B* **771**, 359 (2017), [arXiv:1703.08170 \[hep-ph\]](#).
- [30] D. Bigi, P. Gambino, and S. Schacht, *Phys. Lett. B* **769**, 441 (2017), [arXiv:1703.06124 \[hep-ph\]](#).
- [31] R. Glattauer *et al.* (Belle Collaboration), *Phys. Rev. D* **93**, 032006 (2016), [arXiv:1510.03657 \[hep-ex\]](#).
- [32] E. Waheed *et al.* (Belle Collaboration), *Phys. Rev. D* **100**, 052007 (2019), [arXiv:1809.03290 \[hep-ex\]](#).
- [33] F. U. Bernlochner and Z. Ligeti, *Phys. Rev. D* **95**, 014022 (2017), [arXiv:1606.09300 \[hep-ph\]](#).
- [34] M. Feindt, F. Keller, M. Kreps, T. Kuhr, S. Neubauer, D. Zander, and A. Zupanc, *Nucl. Instrum. Meth. A* **654**, 432 (2011), [arXiv:1102.3876 \[hep-ex\]](#).
- [35] T. Chen and C. Guestrin, *Proceedings of the 22nd ACM SIGKDD International Conference on Knowledge Discovery and Data Mining KDD '16*, 785 (2016).
- [36] Y. Aoki *et al.* (Flavour Lattice Averaging Group (FLAG)), *Eur. Phys. J. C* **82**, 869 (2022), [arXiv:2111.09849 \[hep-lat\]](#).
- [37] J. A. Bailey *et al.* (Fermilab Lattice and MILC Collaborations), *Phys. Rev. D* **92**, 014024 (2015), [arXiv:1503.07839 \[hep-lat\]](#).
- [38] J. M. Flynn, T. Izubuchi, T. Kawanai, C. Lehner, A. Soni, R. S. Van de Water, and O. Witzel, *Phys. Rev. D* **91**, 074510 (2015), [arXiv:1501.05373 \[hep-lat\]](#).
- [39] P. del Amo Sanchez *et al.* (BaBar Collaboration), *Phys. Rev. D* **83**, 032007 (2011), [arXiv:1005.3288 \[hep-ex\]](#).
- [40] J. P. Lees *et al.* (BaBar Collaboration), *Phys. Rev. D* **86**, 092004 (2012), [arXiv:1208.1253 \[hep-ex\]](#).
- [41] H. Ha *et al.* (Belle Collaboration), *Phys. Rev. D* **83**, 071101 (2011), [arXiv:1012.0090 \[hep-ex\]](#).
- [42] A. Sibidanov *et al.* (Belle Collaboration), *Phys. Rev. D* **88**, 032005 (2013), [arXiv:1306.2781 \[hep-ex\]](#).
- [43] R. Aaij *et al.* (LHCb Collaboration), *Eur. Phys. J. C* **74**, 2888 (2014), [arXiv:1402.4430 \[hep-ex\]](#).
- [44] M. Althoff *et al.* (TASSO Collaboration), *Z. Phys. C* **27**, 27 (1985).
- [45] W. Bartel *et al.* (JADE Collaboration), *Z. Phys. C* **20**, 187 (1983).
- [46] P. Gambino, P. Giordano, G. Ossola, and N. Uraltsev,

- JHEP **10**, 058 (2007), [arXiv:0707.2493 \[hep-ph\]](#).
- [47] J. Charles *et al.* (CKMfitter Group), [Eur. Phys. J. C](#) **41**, 1 (2005), and updates of Spring 2021 on <http://ckmfitter.in2p3.fr/>, [arXiv:0406184 \[hep-ph\]](#).
- [48] See the supplemental material at [link provided by PRL].

SUPPLEMENTAL MATERIAL

Determinations with alternative inclusive calculations for the partial rate

Figure 4 compares the inclusive $|V_{ub}|$ values obtained from the GGOU calculation versus BLNP and DGE, respectively.

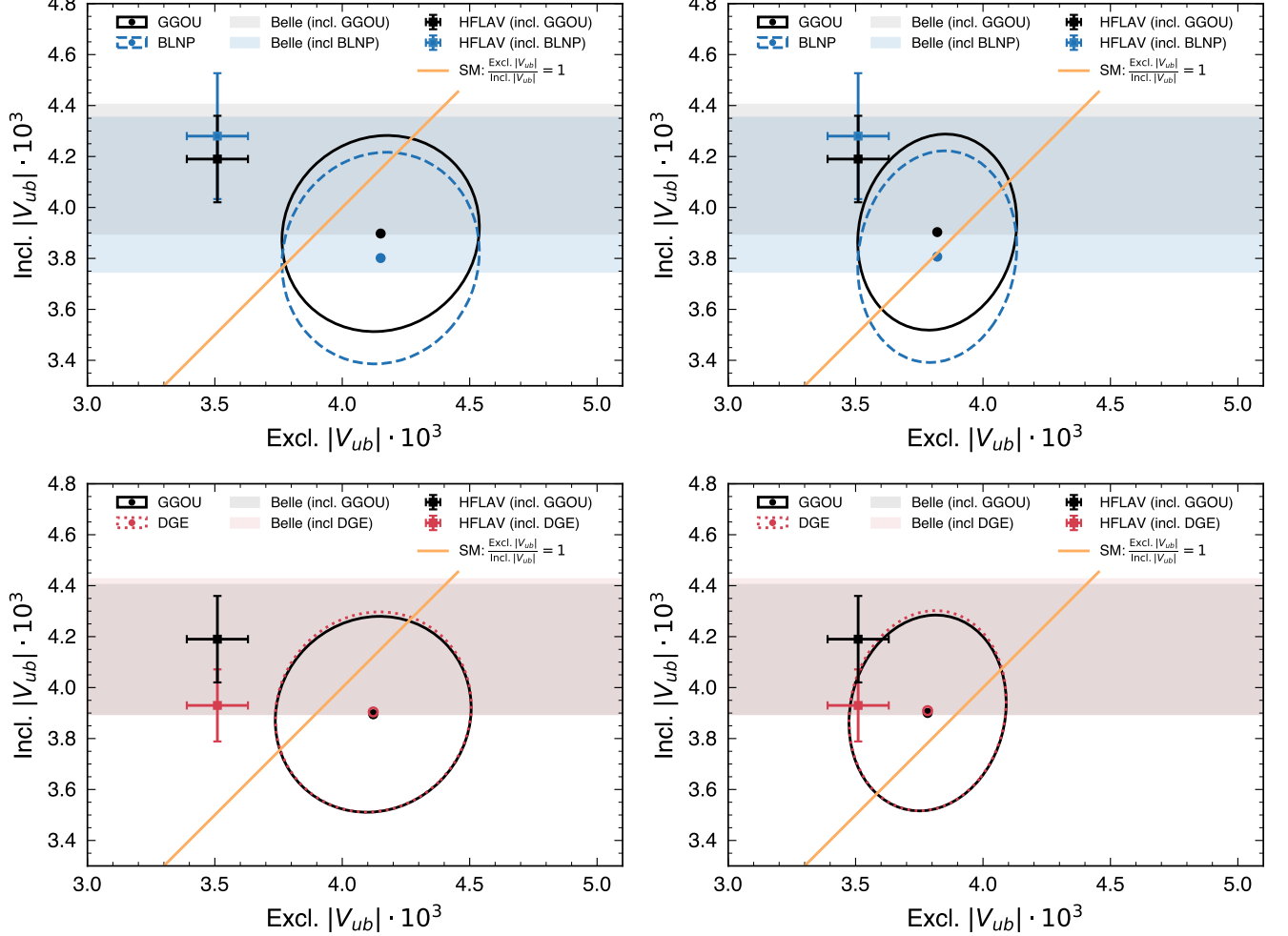


FIG. 4. The $|V_{ub}|$ values obtained using the different theoretical inclusive decay rates are compared: GGOU versus BLNP (up) and GGOU versus DGE (low). The left column shows the fit with only LQCD constraints and the results from combined LQCD-experimental constraints are in the right column.

Data-MC agreement in background dominated sideband

Figure 5 shows the analyzed categories in $q^2 : N_{\pi^\pm}$ for $M_X < 1.7 \text{ GeV}$ and the four $M_X \geq 1.7 \text{ GeV}$ bins in the $B \rightarrow X_c \ell \bar{\nu}_\ell$ enriched BDT sideband. We observe fair agreement in the background shapes with a p-value of 87%.

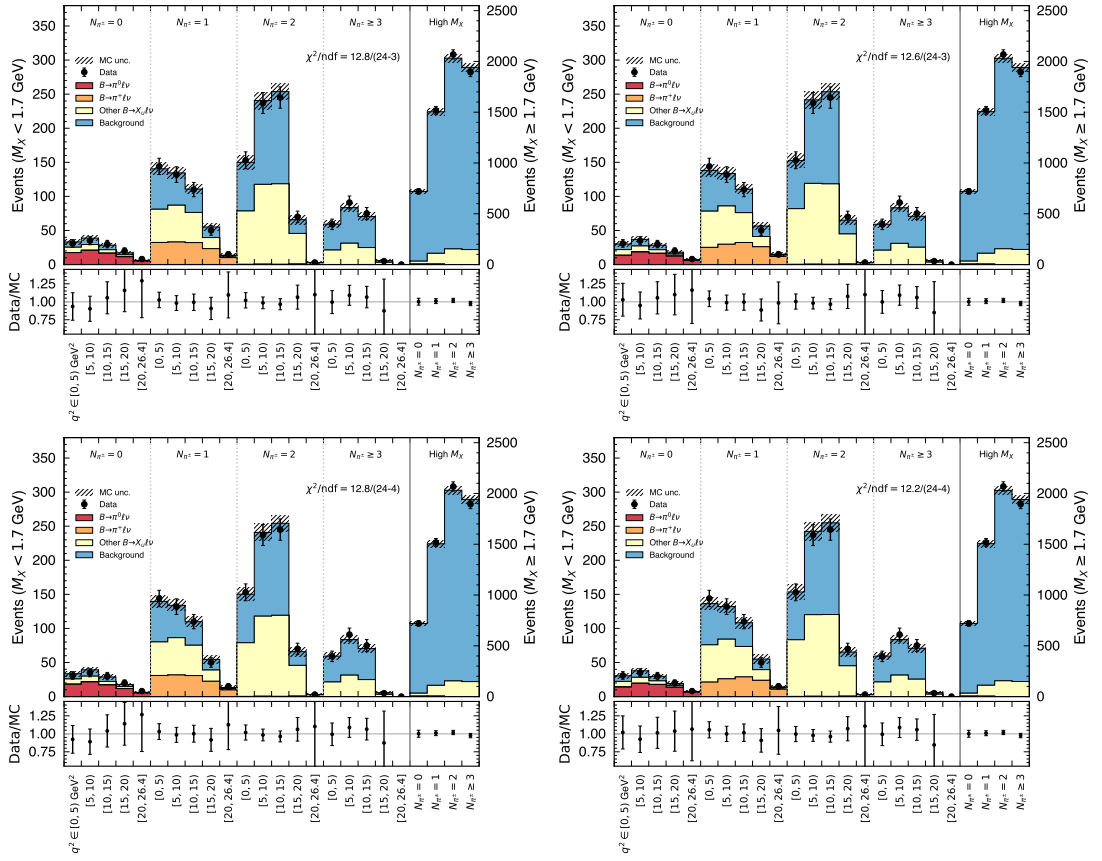


FIG. 6. The postfit $q^2 : N_{\pi^\pm}$ spectra with various setups. From top left to bottom right, the results are shown for the setup 1-a, 1-b, 2-a and 2-b. The uncertainties incorporate all post-fit uncertainties discussed in the main text.

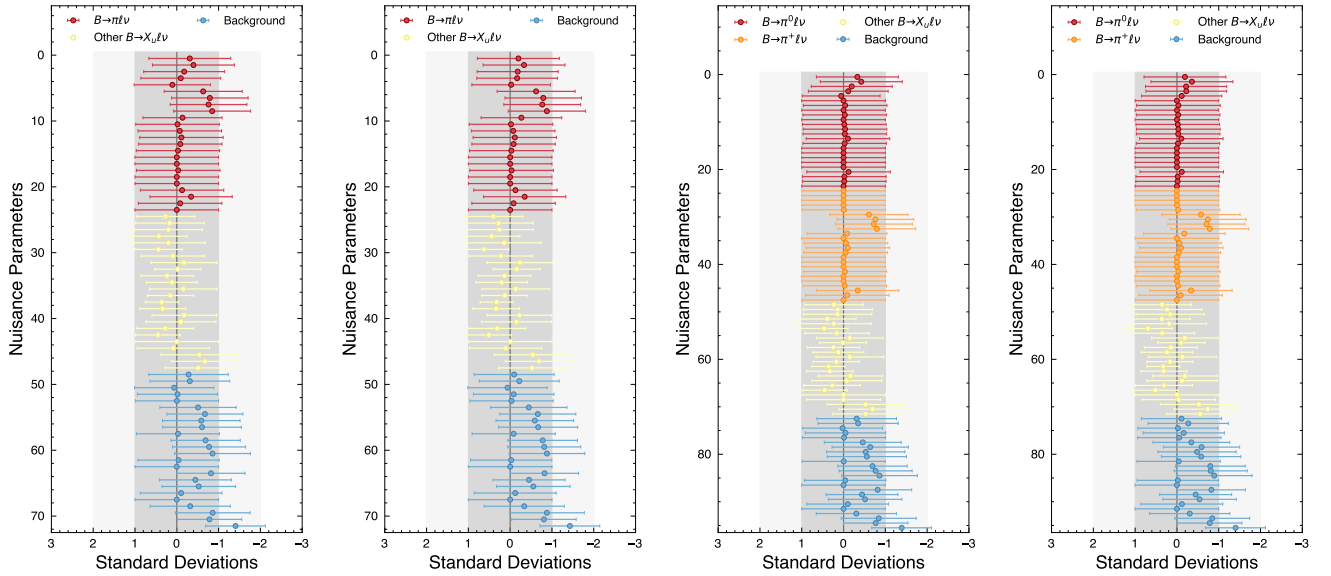


FIG. 7. The pulls of Nuisance parameters. From left to right, the results are shown for the setup 1-a, 1-b, 2-a and 2-b. The uncertainty of each pull shows the post-fit error normalized to the pre-fit constraint.

Setup	$B^+ \rightarrow \pi^0 \ell^+ \nu_\ell$	$B^0 \rightarrow \pi^- \ell^+ \nu_\ell$	Other $B \rightarrow X_u \ell \bar{\nu}_\ell$	Bkg.
1-a	78 ± 11	147 ± 21	1087 ± 241	7209 ± 631
1-b	72 ± 11	143 ± 23	1095 ± 241	7226 ± 631
2-a	80 ± 14	141 ± 31	1089 ± 241	7200 ± 631
2-b	77 ± 14	125 ± 32	1104 ± 241	7205 ± 632
$10^3 \cdot \epsilon_{\text{sig}}$	0.30	0.32	0.26	-

TABLE I. The fitted yields for $B^+ \rightarrow \pi^0 \ell^+ \nu_\ell$, $B^0 \rightarrow \pi^- \ell^+ \nu_\ell$, other $B \rightarrow X_u \ell \bar{\nu}_\ell$ decays and backgrounds with various fitter setups. The uncertainties assigned to the fitted yields include the statistical and systematic impacts in the fitting procedure. The signal efficiencies ϵ_{sig} are also listed.

Result	
Setup 1-a	
$ V_{ub} ^\pi$	$(3.78 \pm 0.23 \pm 0.16 \pm 0.14) \times 10^{-3}$
$ V_{ub} ^{\text{incl.}}$	$(3.90 \pm 0.20 \pm 0.32 \pm 0.09) \times 10^{-3}$
$ V_{ub} ^\pi / V_{ub} ^{\text{incl.}}$	0.97 ± 0.12
$\rho(V_{ub} ^\pi, V_{ub} ^{\text{incl.}})$	0.10
Setup 1-b	
$ V_{ub} ^\pi$	$(4.12 \pm 0.30 \pm 0.18 \pm 0.16) \times 10^{-3}$
$ V_{ub} ^{\text{incl.}}$	$(3.90 \pm 0.20 \pm 0.32 \pm 0.09) \times 10^{-3}$
$ V_{ub} ^\pi / V_{ub} ^{\text{incl.}}$	1.06 ± 0.14
$\rho(V_{ub} ^\pi, V_{ub} ^{\text{incl.}})$	0.07

TABLE II. The determined $|V_{ub}|$ results and various ratios with the setup 1-a and 1-b, respectively.

BCL parameters of $B \rightarrow \pi \ell \bar{\nu}_\ell$ decay form factor

The fitted BCL parameters are summarized in Table VI and VII with only LQCD constraints and combined LQCD-experimental constraints, respectively. Figure 8 compares the results obtained in various fit scenarios, which are in good agreement.

Result	
Setup 1-a	
$\mathcal{B}(B^0 \rightarrow \pi^- \ell^+ \nu_\ell)$	$(1.53 \pm 0.18 \pm 0.12) \times 10^{-4}$
$\Delta\mathcal{B}(B \rightarrow X_u \ell \bar{\nu}_\ell)$	$(1.40 \pm 0.14 \pm 0.23) \times 10^{-3}$
$\rho(\mathcal{B}^\pi, \Delta\mathcal{B}^{X_u})$	0.12
Setup 1-b	
$\mathcal{B}(B^0 \rightarrow \pi^- \ell^+ \nu_\ell)$	$(1.43 \pm 0.19 \pm 0.13) \times 10^{-4}$
$\Delta\mathcal{B}(B \rightarrow X_u \ell \bar{\nu}_\ell)$	$(1.40 \pm 0.14 \pm 0.23) \times 10^{-3}$
$\rho(\mathcal{B}^\pi, \Delta\mathcal{B}^{X_u})$	0.10

TABLE III. The measured branching fractions and various correlations based on the setup 1-a and 1-b, respectively.

Result	
Setup 2-a	
$ V_{ub} ^{\pi^0}$	$(3.87 \pm 0.30 \pm 0.18 \pm 0.15) \times 10^{-3}$
$ V_{ub} ^{\pi^+}$	$(3.70 \pm 0.34 \pm 0.23 \pm 0.10) \times 10^{-3}$
Avr. $ V_{ub} ^{\pi}$	$(3.79 \pm 0.31) \times 10^{-3}$
$ V_{ub} ^{\text{incl.}}$	$(3.90 \pm 0.20 \pm 0.31 \pm 0.09) \times 10^{-3}$
$ V_{ub} ^{\pi}/ V_{ub} ^{\text{incl.}}$	0.97 ± 0.12
$\rho(V_{ub} ^{\pi}, V_{ub} ^{\text{incl.}})$	0.10
$\rho(V_{ub} ^{\pi^+}, V_{ub} ^{\pi^0})$	0.20
Setup 2-b	
$ V_{ub} ^{\pi^0}$	$(4.40 \pm 0.44 \pm 0.25 \pm 0.17) \times 10^{-3}$
$ V_{ub} ^{\pi^+}$	$(3.93 \pm 0.37 \pm 0.24 \pm 0.14) \times 10^{-3}$
Avr. $ V_{ub} ^{\pi}$	$(4.13 \pm 0.39) \times 10^{-3}$
$ V_{ub} ^{\text{incl.}}$	$(3.89 \pm 0.20 \pm 0.32 \pm 0.09) \times 10^{-3}$
$ V_{ub} ^{\pi}/ V_{ub} ^{\text{incl.}}$	1.06 ± 0.14
$\rho(V_{ub} ^{\pi}, V_{ub} ^{\text{incl.}})$	0.06
$\rho(V_{ub} ^{\pi^+}, V_{ub} ^{\pi^0})$	0.25

TABLE IV. The determined $|V_{ub}|$ results and various ratios based on the setup 2-a and 2-b, respectively.

Result	
Setup 2-a	
$\mathcal{B}(B^+ \rightarrow \pi^0 \ell^+ \nu_\ell)$	$(0.85 \pm 0.13 \pm 0.08) \times 10^{-4}$
$\mathcal{B}(B^0 \rightarrow \pi^- \ell^+ \nu_\ell)$	$(1.47 \pm 0.26 \pm 0.18) \times 10^{-4}$
$\Delta\mathcal{B}(B \rightarrow X_u \ell \bar{\nu}_\ell)$	$(1.40 \pm 0.15 \pm 0.23) \times 10^{-3}$
$\rho(\mathcal{B}^{\pi^0}, \mathcal{B}^{\pi^+})$	0.08
$\rho(\mathcal{B}^{\pi^0}, \Delta\mathcal{B}^{X_u})$	0.08
$\rho(\mathcal{B}^{\pi^+}, \Delta\mathcal{B}^{X_u})$	0.08
Setup 2-b	
$\mathcal{B}(B^+ \rightarrow \pi^0 \ell^+ \nu_\ell)$	$(0.83 \pm 0.13 \pm 0.08) \times 10^{-4}$
$\mathcal{B}(B^0 \rightarrow \pi^- \ell^+ \nu_\ell)$	$(1.26 \pm 0.27 \pm 0.17) \times 10^{-4}$
$\Delta\mathcal{B}(B \rightarrow X_u \ell \bar{\nu}_\ell)$	$(1.40 \pm 0.14 \pm 0.23) \times 10^{-3}$
$\rho(\mathcal{B}^{\pi^0}, \mathcal{B}^{\pi^+})$	0.15
$\rho(\mathcal{B}^{\pi^0}, \Delta\mathcal{B}^{X_u})$	0.08
$\rho(\mathcal{B}^{\pi^+}, \Delta\mathcal{B}^{X_u})$	0.05

TABLE V. The measured branching fractions and various correlations based on the setup 2-a and 2-b, respectively.

	$ V_{ub} \times 10^3$	a_0^+	a_1^+	a_2^+	a_0^0	a_1^0
Central	4.122	0.406	-0.615	-0.550	0.494	-1.527
Uncertainty	0.384	0.012	0.082	0.401	0.020	0.098
$ V_{ub} $	1.000	-0.419	-0.486	-0.328	-0.191	-0.478
a_0^+		1.000	0.274	-0.177	0.255	0.174
a_1^+			1.000	0.371	0.109	0.731
a_2^+				1.000	0.200	0.712
a_0^0					1.000	-0.027
a_1^0						1.000

TABLE VI. The measured $B \rightarrow \pi \ell \nu$ form factor BCL parameters and exclusive $|V_{ub}|$ with full correlations. The shape of q^2 is constrained by the LQCD fit results from FLAG.

	$ V_{ub} \times 10^3$	a_0^+	a_1^+	a_2^+	a_0^0	a_1^0
Central	3.783	0.414	-0.494	-0.297	0.500	-1.426
Uncertainty	0.308	0.014	0.053	0.180	0.023	0.054
$ V_{ub} $	1.000	-0.453	-0.171	0.232	-0.109	-0.106
a_0^+		1.000	0.152	-0.451	0.259	0.142
a_1^+			1.000	-0.798	-0.096	0.215
a_2^+				1.000	0.012	-0.097
a_0^0					1.000	-0.451
a_1^0						1.000

TABLE VII. The measured $B \rightarrow \pi \ell \nu$ form factor BCL parameters and exclusive $|V_{ub}|$ with full correlations. The shape of q^2 is constrained by the combined LQCD and experimental fit results from FLAG.

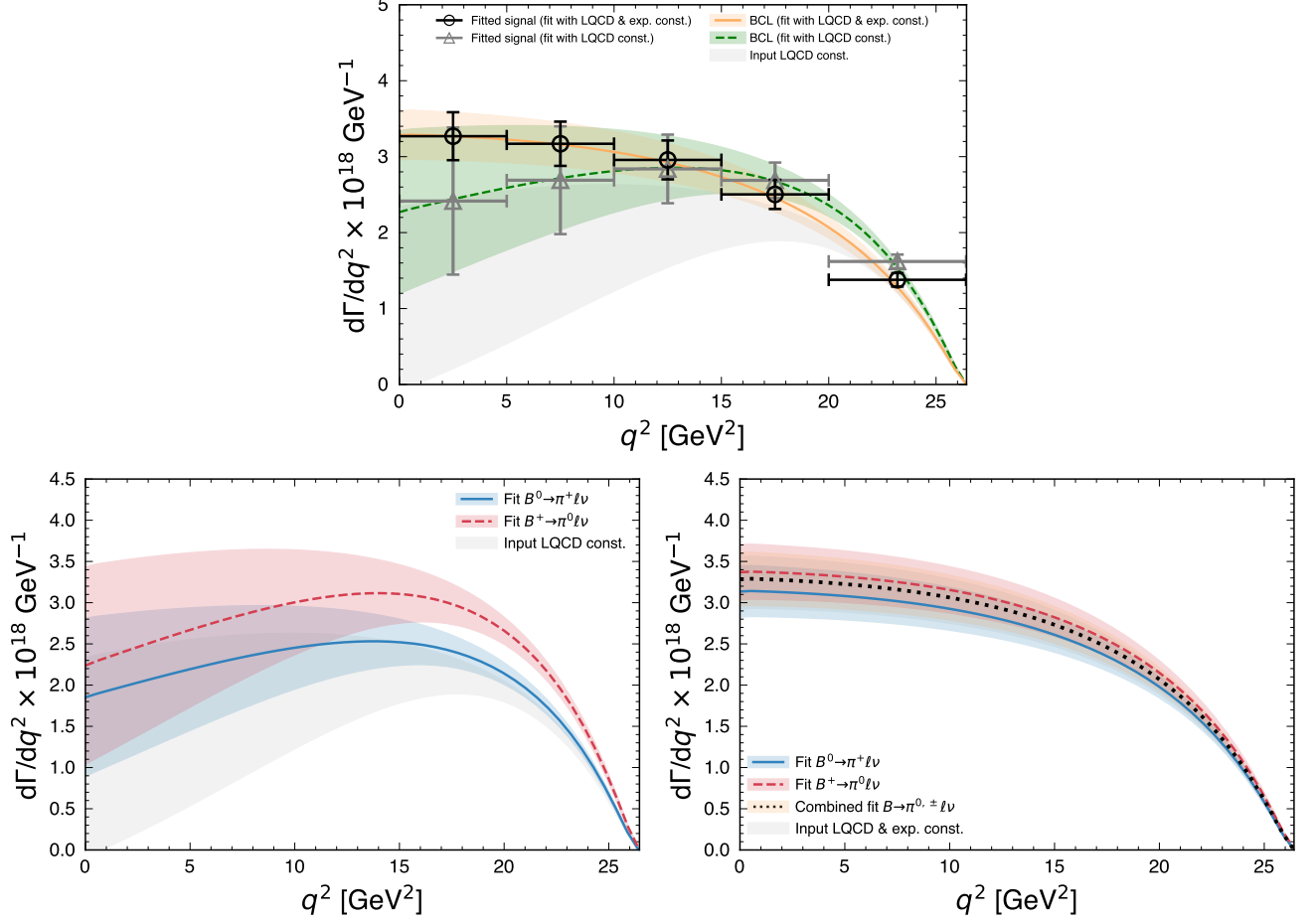


FIG. 8. Top: the q^2 spectra of $B \rightarrow \pi \ell \bar{\nu}_\ell$ obtained from the fit of the combined LQCD and experimental information (orange, solid) and from the fit to LQCD only (green, dashed) are shown. The data points are the post-fit signal distributions, corrected for resolution and efficiency effects and averaged over both isospin modes. The input LQCD constraints from FLAG are shown in grey. Bottom left: the q^2 spectra obtained with separated (blue, solid) π^+ mode and (red, dashed) π^0 using the LQCD only information from FLAG to constrain the $B \rightarrow \pi \ell \bar{\nu}_\ell$ form factor (setup 2-b). Bottom right: the results obtained by using the LQCD and experimental constraint (setup 2-a). The combined fit (setup 1-a) result is shown for comparison (black, dotted).